International Journal of Automotive Technology, Vol. 4, No. 4, pp. 173–180 (2003)

Article No. 1229–9138/2003/14–03

UNMANNED VEHICLE CONTROL AND MODELING FOR OBSTACLE AVOIDANCE

S. G. KIM and J. H. KIM*

Graduate School of Automotive Engineering, Kookmin University, Seoul 136-702, Korea

(Received 19 April 2003; Revised 24 September 2003)

ABSTRACT–Obstacle avoidance is considered as one of the key technologies in an unmanned vehicle system. In this paper, we propose a method of obstacle avoidance, which can be expressed as vehicle control, modeling, and sensor experiments. Obstacle avoidance consists of two parts: one longitudinal control system for acceleration; and deceleration and a lateral control system for steering control. Each system is used for unmanned vehicle control, which notes its location, recognizes obstacles surrounding it, and makes a decision how fast to proceed according to circumstances. During the operation, the control strategy of the vehicle can detect obstacles and perform obstacle avoidance on the road, which involves vehicle velocity. The method proposed for vehicle control, modeling, and obstacle avoidance has been confirmed through vehicle tests.

KEY WORDS : Unmanned vehicle, Lateral control, Longitudinal control, Obstacle avoidance, Ultrasonic sensor, Laser scanner

1. INTRODUCTION

During the past decade considerable effort has been made to develop an unmanned vehicle for applications in the military, surveillance, terrain mapping and emergency environment, and vehicle safety, and this effort has recently been associated with social infrastructure (Kim, 2001). Also, most unmanned vehicles use variable sensors for vehicle safety and accurate vehicle control. Therefore, research into hardware and software control is very important for vehicle operation. Recently, research of most vehicles has been focused on the vehicle stability and customer satisfaction, including riding convenience, reduced emission, and fuel-efficient advantage.

In this paper, we propose motion control and modeling for the unmanned vehicle control and obstacle avoidance, which require accuracy and sensitivity. Therefore, we used accurate sensors, such as an ultrasonic sensor, laser scanner, the wireless communication module, which are very important for the operation of an unmanned vehicle. Finally, in this research, we presented vehicle modeling for the traction and the steering control and it is confimed by simulation and vehicle test. Additionally, obstacle avoidance was evaluated by an ultrasonic sensor and a laser scanner.

*Corresponding author. e-mail: jhkim@kookmin.ac.kr

2. VEHICLE CONTROL SYSTEM OF AN UNMANNED VEHICLE

2.1. Longitudinal Control

In the research, the longitudinal control of a vehicle is operated by a motor and brake control. The motor driving system is controlled by the input voltage to the motor by digital signal processing and conversion to an analog signal via a D/A converter (Lee, 2001).

The vehicles velocity is calculated from the wheel rotation, which is measured by counting a Hall sensor signal. The velocity data use total vehicle moving distance calculation, which also is used as a velocity profile for path planning. The traction motor controller is used for the vehicle driving control through a traction motor. It is controlled by a voltage signal to the motor rotation so it generates the driving torque, which causes wheel rotation. Consequently, the vehicle velocity and distance are calculated from the wheel rotation counter.

Driving system modeling

In the research, we used the DC motor modeling for vehicle control of longitudinal distance. It directly provided rotary motion and, coupled with wheels or drums and cables provided transitional motion. The electric circuit of the armature and the free body diagram of the rotor are shown in Figure 1 (Kim, 1993; Paresh, 1998). The control objective was determined by vehicle

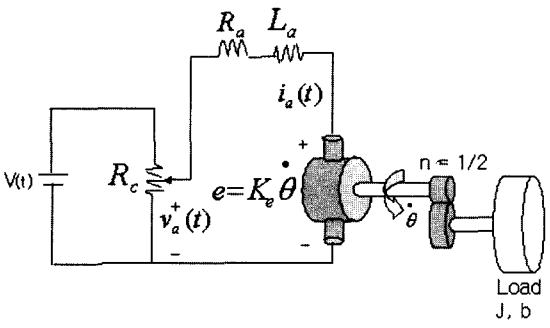

Figure 1. Wire model of driving system.

velocity and safe distance maintenance (Kim, 2001).

The armature voltage of the motor-electro approval, v_a(t) is controlled proportionally to the source voltage $V(t)$ of the equal circuit, where $i_a(t)$ is the armature current, R_a is the electric resistance, L_a is the electric inductance component of the electric windings, and e is a counter-electromotive force conduction of electricity while the motor is rotating. From the figure above we can write the following equations based on Newton's law combined with Kirchhoff's law. The torque T can be written, as in Equation (1), where J is the moment inertia of the motor, b is damping ratio of the mechanical system, and k_t is the armature constant.

$$T = k_t i_a = J\frac{d\dot{\theta}}{dt} + b\dot{\theta} + J\ddot{\theta} + b\dot{\theta} \tag{1}$$

Generally, electric voltage is conducted proportionally by the magnetic velocity and angular velocity as the magnetic field rotates. Therefore, e is related to the rotational velocity by the following equations.

$$e = k_e\dot{\theta}. \tag{2}$$

Where k_e is the counter-electromotive force constant. The voltage equation of the equivalent circuit is related by the following equations.

$$V(t) = k_a v_a(t) \tag{3}$$

$$v_a(t) - e = R_a i_a + L_a\frac{di_a}{dt} \tag{4}$$

Where electric resistance R_a and counter-electromotive force k_a are constant, and it is assumed that all initial conditions are zero. Using Laplace Transforms of the above modeling equations, we get the following transfer function, where the rotating speed is the output and the voltage is an input.

$$\frac{\Theta(s)}{V(s)} = \frac{k_a k_t}{(R_a + L_a s) + (Js + b) + k_t k_e} \tag{5}$$

Figure 2 shows the system closed-loop block diagram

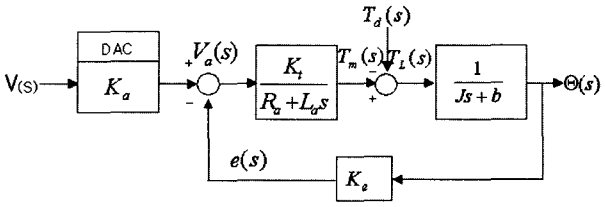

Figure 2. Closed-loop block diagram of traction system.

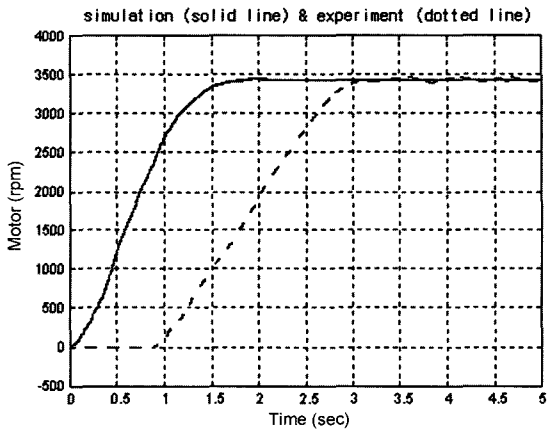

Figure 3. Comparison of DC motor transfer function between experiment and simulation results.

of transfer function of Equation (5).

Exact values for the motor rotor inertia, electric resistance, and electric inductance values are difficult to determine. Therefore, this research has determined the transfer function through iterative experiments as an approximate value (Franklin, 1995). Figure 3 shows the motor velocity profile for a step input voltage and the simulation result of the transfer function, which is expressed in the MATLAB program m-file to verify the transfer function. This experiment was performed using the *Lab-View* software (National, 1996).

We have found the natural frequency and damping ratio, which are used to get the transfer function. The traction function of the traction system can be rewritten as Equation (6).

$$G(s) = \frac{\Theta(s)}{V(s)} = \frac{5866.575}{s^2 + 4.55s + 7.111} \tag{6}$$

2.2. Lateral Control

The steering actuator for accurate steering control uses a stepping motor, which uses a timing belt to connect with the steering column.

The steering torque of the steering column is estimated by a torque measurer, which required about 20[Kg·cm]. Therefore, in this experiment we chose a stepping motor

(PK-296 model) to overcome the force of reaction that has a 1400[g·cm^2] rotor inertia moment and a maximum holding torque of 22[Kg·cm]. This stepping motor torque is controlled by a 10:1 reduced gear ratio. The experimental results show that total steering angle is 1080 degrees and the total number of pulses is 12,000. So, factor (α) of the relationship input pulse and the steering angle is defined as

$$\alpha = \frac{360^\circ}{4000}\ [\text{deg/}pulse] = 0.09[\text{deg/}pulse]$$
$$\frac{1}{4000}\ [rev/pulse] = 0.00025[rev/pulse] \quad (7)$$

In Equation (7), we know the maximum resolution is about 0.18 degree.

Steering system modeling

The bicycle model is used for a precise and improved steering system of an unmanned vehicle. We considered that the vehicle has to disregard the rolling motion on normal road conditions and driving constant velocity. If the vehicle, moving on a flat road, has acceleration on the lateral side, the acceleration occurs about the normal direction and the wheel has acceleration, which is the cornering force (Dorf, 1997; Thomas, 1992). Figure 4 shows the dynamic motion parameters of the steering system, which is expressed as the coordinate system for the bicycle model.

If it is assumed that the steering angle of all the front wheels about the vehicle position is δ, the front and rear bilateral wheel sideslip angles of each tire is β_{f1}, β_{f2}, β_{r1}, β_{r2}, and the cornering forces of the tire are Y_{f1}, Y_{f2}, Y_{r1}, Y_{r2} (Park, 2001; Ellis, 1969).

The cornering force of the front and rear tires is assumed to be K_f and K_r. The sideslip angle is positive and applied in a negative direction from the y axis. From the figure above we can write the following equations about bicycle modeling.

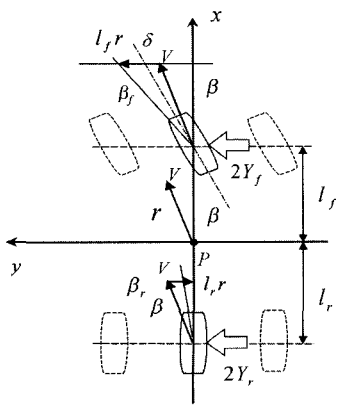

Figure 4. Bicycle model for steering system modeling.

$$mV\frac{d\beta}{dt} + 2(K_f+K_r)\beta + \left\{mV+\frac{2}{V}(l_fK_f-l_rK_r)\right\}r = 2K_f\delta \quad (8)$$

$$2(l_fK_f-l_rK_r)\beta + I\frac{dr}{dt} + \frac{2(l_f^2K_f-l_r^2K_r)}{V}r = 2l_fK_f\delta \quad (9)$$

From Equations (8) and (9), we can lead to motion equation of vehicle yawing angle acceleration. The Laplace transformation yields.

$$\frac{R(s)}{\delta(s)} = \frac{2(mVl_fK_fs + (l_fK_f^2+2K_fK_r(2l_f-l_r))}{mVI\left(s^2+\frac{2m(l_f^2K_f+l_r^2K_r)+2I(K_f+K_r)}{mIV}s+\frac{4K_fK_rV^2}{mIV^2}-\frac{2(l_fK_f-l_rK_r)}{I}\right)} \quad (10)$$

However, the numerical value of the system parameters K_f, K_r, and the vehicle yawing I (the moment of inertia) are difficult to determine. Therefore, in this research, these parameters were determined experimentally. The vehicle is given a step input for the steering angle (δ) and the output rotation value of the vehicle is measured by the gyro sensor.

Figure 5 shows the measured response of the vehicle to a step input and simulation result to the steering angle (δ). The system transfer function of Equation (11) leads to many experiments in Figure 5.

$$G(s) = \frac{R(s)}{\delta(s)} = \frac{97.3}{s^2+2.31s+2.78} \quad (11)$$

The result of the modeling response agrees with the experimentally measured values. However, the result

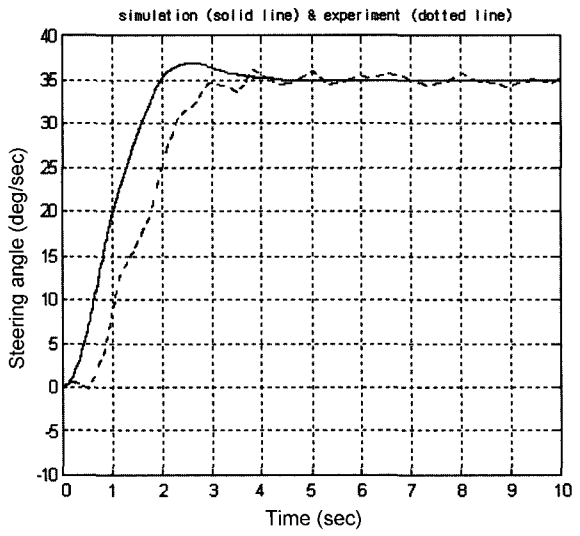

Figure 5. Comparison of steering angle transfer function between experiment and simulation results.

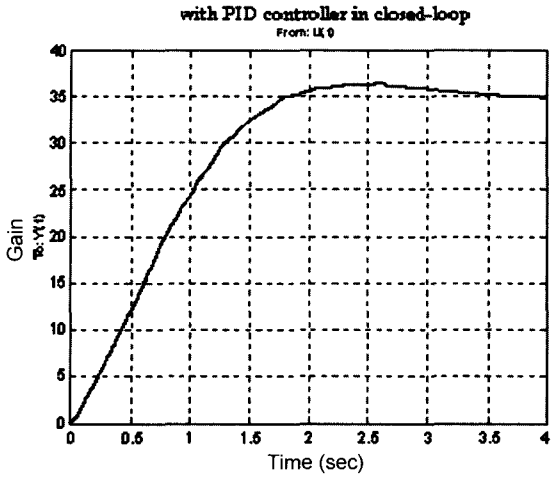

Figure 6. Closed-loop system simulation with PID controller.

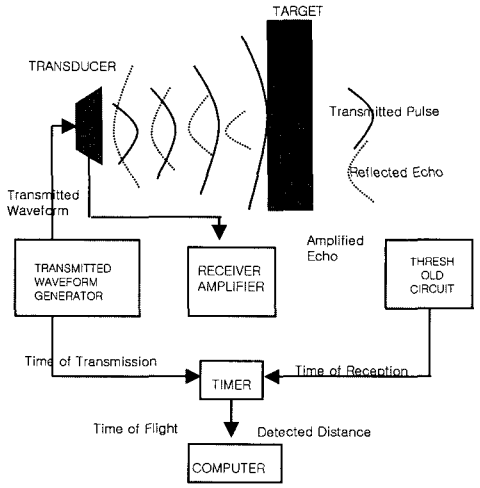

Figure 7. Functional diagram of the ultrasonic sensor.

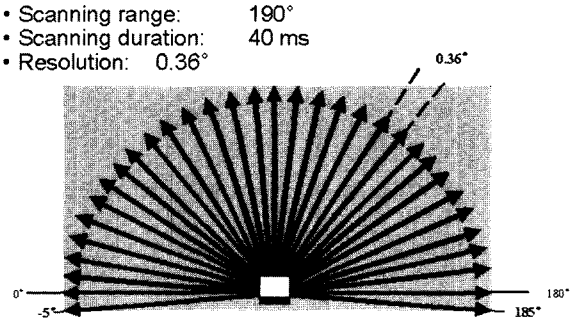

Figure 8. Scanning field of the laser scanner.

does not show accurate agreement with the experimental results due to the noise and incomplete tuning. But the settling time, rising time, and steady-state error are almost similar. More accurate experimental conditions and tuning would make it possible to determine exactly the transfer function for the steering control.

For more precise lateral control, it requires PID controller, and so forth. Equation (12) shows the transfer function of closed loop system, where K_p, K_i, K_d mean PID gain values, individually.

$$G_c(s) = \frac{R(s)}{\delta(s)} = \frac{97.3(K_d s^2 + K_p s + K_i)}{s^3 + (K_d + 2.31)s^2 + (K_p + 2.78)s + K_i} \tag{12}$$

When P gain sets as 2, D gain sets as 1 and I gain sets as 0, the system settling time is diminished to1 second. Figure 6 shows the simulation result based on those gain values.

3. SENSOR SYSTEM OF AN UNMANNED VEHICLE

Ultrasonic Sensor and Laser Scanner

In the research, ultrasonic sensors and laser scanner are used for obstacles detecting and obstacle avoidance when the vehicle is in motion. Generally, the distance measurement signal of the ultrasonic sensor and laser scanner is converted into digital data by an A/D converter, and it calculates distance to the main computer according to a pic-process and DAQ board signal. The distance among the ultrasonic sensor, laser scanner and the obstacle is measured by the ultrasonic sensor and laser scanner principle. Figure 7 shows the principle of the time variable gain amplifier and the functional diagram of the ultrasonic sensor (Tumbo, 2001). Figure 8 shows the scanning field of the laser scanner. Generally, the laser scanner works by measuring the time of flight of laser light pulses. The pulsed laser beam is deflected by an internal rotating mirror so that a fan-shaped scan is made of the surrounding area. The shape of the object is determined by the sequence of impulses received. The scanners measurement data can be individually processed in real time with external evaluation software. Standard solutions are also available for object measurement. The unit communicates with the host computer using an RS232 serial interface card.

4. TEST EVALUATION

Obstacle detection and avoidance experiment estimation are one of the foremost experiments in unmanned vehicles. Generally, the ultrasonic sensor is one of the range sensors, which can measure a distance to objects, and it is more commonly used with an unmanned vehicle

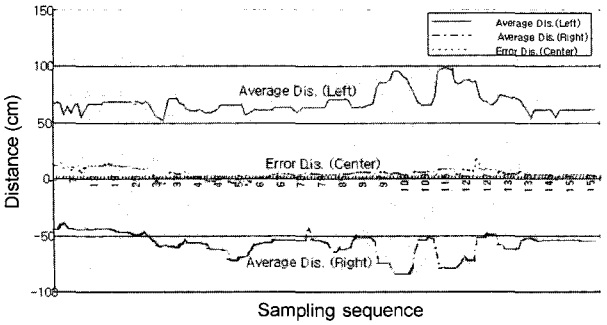

Figure 9. Ultrasonic sensor experimental result in corridor (Average and error rate).

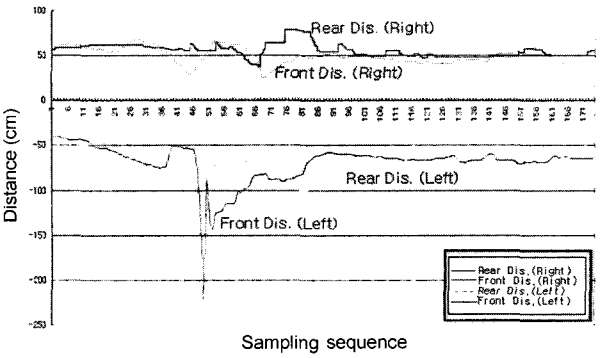

Figure 11. Ultrasonic sensor experimental result in corridor (Compare sensor S-turn signal).

and mobile robots because it is small, inexpensive, and it is easy to calculate the object's distance. In this research, we used the ultrasonic sensor made by the Senix Company (ULTRA-U) (Kim *et al.*, 2001). We attached sensors to both sides and front in the vehicle for ultrasonic sensor and laser scanner characteristic analysis and a collision avoidance test. They can detect the front and side objects (Lee, 1999).

The first experiment stage is environment detecting by the corridor and finding the center position of bilateral wall with the ultrasonic sensor and laser scanner. The test result of the ultrasonic sensor shows in Figure 9, and it shows average distance values from the centerline of the corridor to the wall and the sensor error rate from the centerline to the wall.

Figure 10 is shown comparision of the test result values of the ultrasonic sensors. Four sensors are used for this experiment. Two of those are mounted in front and others are rear of both sides. Each of the sensor's signal measures a distance between the vehicle and corridor wall, and each curve shows a state of the corridor wall. We know from the results that it is only a small-time delay and it shows a similar trend from the sensor signal.

As the result of another experiment, Figure 11 compares

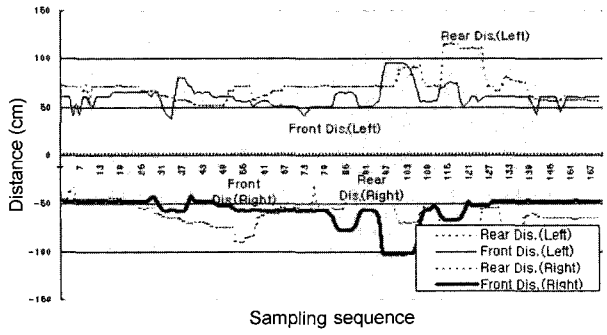

Figure 10. Ultrasonic sensor experimental result in corridor (Compare sensor signal).

the test results of S-turn driving under the same conditions. We know from the results that it is only a small-time delay and it shows a similar trend from the sensor signal.

Figures 12 and 13 show a series of experimental runs of laser scanner in the corridor. In each case, the scanner look-ahead distance was between 2m and 3m. From the result of first experimental, we see one spike in the field of view. One chair is closer to the scanner. Now the scanner just sees the one chair as it has a dimensional field of view

Figure 13 shows a person standing in the center in front of the vehicle to see the difference in the field of view. When we see him in the field of view, we see him as one object. At the height of the laser scanner, he will be seen as one object. The shape of the curve shows how accurately the laser scanner gives us data. One man is closer to the scanner. Now the scanner sees just the one obstacle of the one man as it has a dimensional field of view.

The second experiment concerns the object avoidance method of an ultrasonic sensor. Figure 14 shows the test

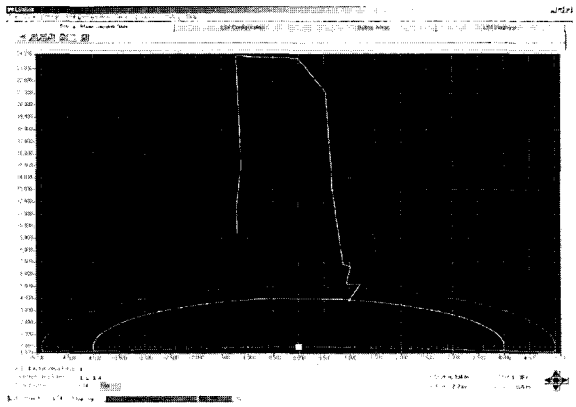

Figure 12. Screen shot with one chair in the field of view.

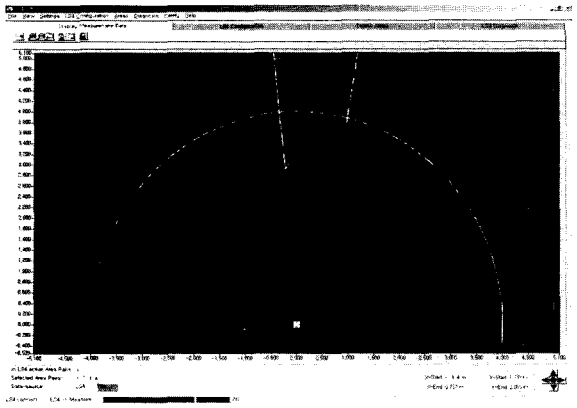

Figure 13. Screen shot with one person in the field of view.

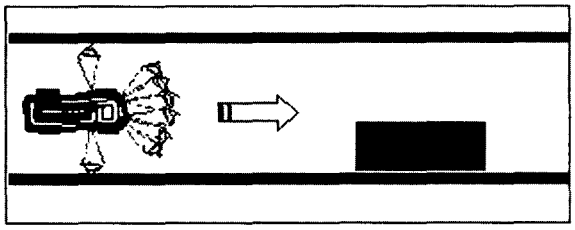

Figure 14. Environment of road, which has an obstacle in the front.

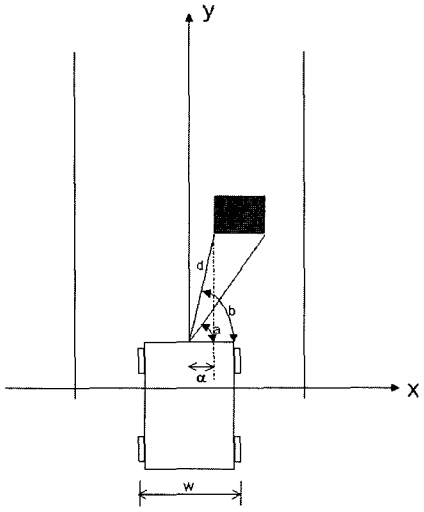

Figure 15. Obstacle on the right of the vehicle.

environment on the road, which has an obstacle in the front.

Figures 15 and 16 show the method of the obstacle avoidance in the Figure 14 condition.

If obstacle on the right of the vehicle, it is described as

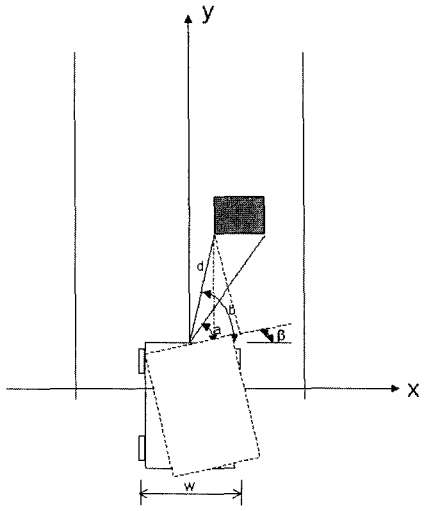

Figure 16. Obstacle avoidance by turning an angle (β).

following step. (condition, a < 90° and b < 90°)

(1) Check if vehicle can maintain same path and avoid obstacle without offsetting the centroid of the vehicle from the center of the track.
(2) $\alpha = d^*Cos(b)$ and $\alpha > 1/2w$ it can continue on straight path without offsetting vehicle centroid.
(3) When $\alpha = d^*Cos(b)$ and $\alpha <= 1/2w$ Calculate steering angle (β) that the vehicle has to turn such that αnew = (1/2w+safety factor) where safety factor = 1 ft.
(4) Vehicle starts turning left and continues turning left till $d^*Cos(b-\beta) = \alpha new$ and β is the steering angle vehicle has turned from its original position.
(5) The vehicle now starts to turn right to maintain its centroid along a path parallel to the centerline of the track and offset by a distance of $\alpha new - \alpha old$.
(6) Thus the hugging distance (the distance of the vehicle from the centroid of the road followed) is calculated as the previous hugging distance ± the offset.

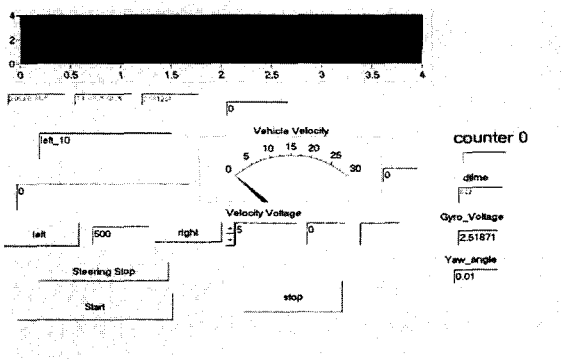

Figure 17. Display of detecting obstacle and avoidance.

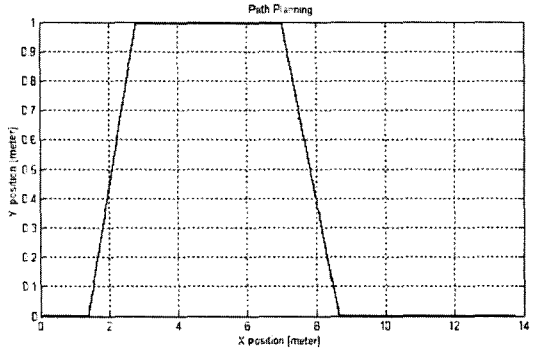

Figure 18. The experimental result of the path planning.

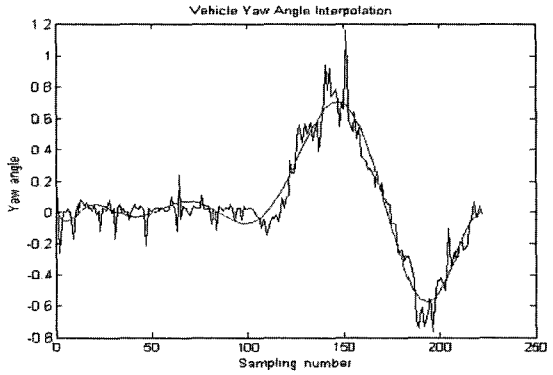

Figure 19. Interpolation curve result of yaw angle.

Figures 17 and 18 show the display software to detect an obstacle and the result of the path planning, which see all the necessary information about the object, such as size, data, and environment (road) profile.

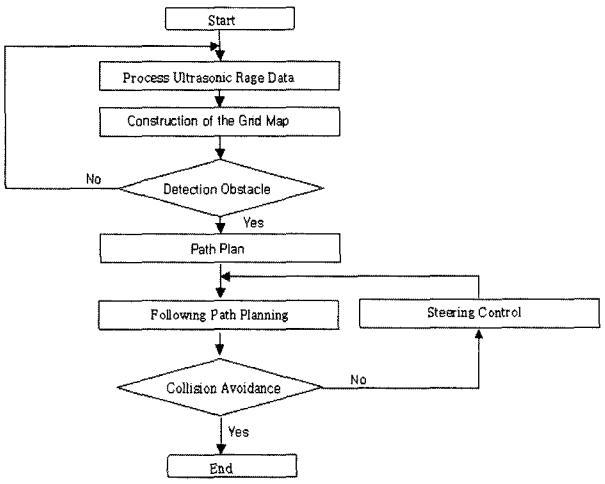

Figure 20. The flowchart of the obstacle avoidance algorithm.

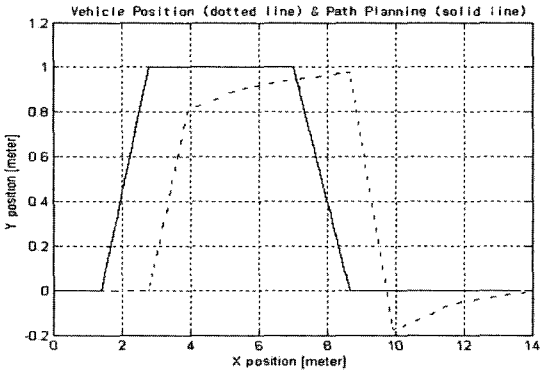

Figure 21. Comparison between vehicle position and path planning.

Figure 19 shows the vehicle is vehicle's yaw angle of interpolation for obstacle detection or collision avoidance, and it shows spline graphics by gyroscope and ultrasonic sensor input data.

Figures 20 and 21 show the algorithm of the obstacle avoidance and comparison between vehicle position and path planning according to the vehicle driving.

From Figure 21, we knew that it is similar trend of the vehicle trajectory and path plan. Also, steering control law of the vehicle for obstacle avoidance shows through the algorithm flowchart.

The vehicle is yaw angle interpolation versus the steering input graphic is shown in Figure 22. The interpolation curve by gyroscope and ultrasonic sensor input data is the reverse of the steering input data curve. Figure 23 shows the collision avoidance trajectory for an unmanned vehicle in the Figure 14 condition, which used an ultrasonic sensor and laser scanner algorithm for reducing the calculation time and error rate. The vehicle trajectory of collision avoidance is larger than the minimum radius of the target trajectory because the ultrasonic sensors and laser scanner are giving an

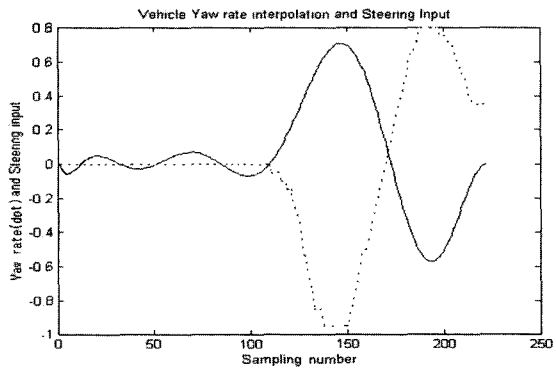

Figure 22. Vehicle yaw angle interpolation versus steering input.

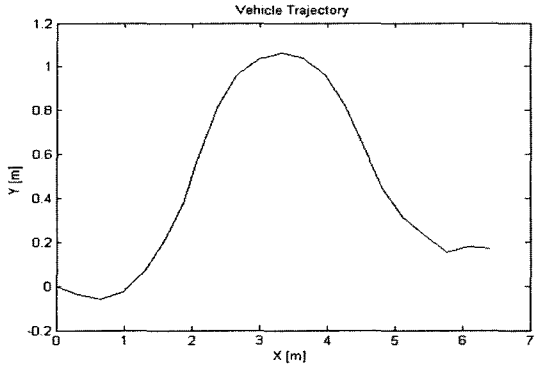

Figure 23. Vehicle trajectory of collision avoidance.

unstable signal output on the vehicle experiment. This problem can be solved by using ultrasonic sensor signal filtering and developing the more advanced control algorithm, such as PID control and fuzzy logic.

5. CONCLUSIONS

In this research, we showed the modeling and design analysis of a utility unmanned vehicle system for autonomous vehicle control. The designed unmanned vehicle system can be operated by sensors, actuators, and possibly a controller, as well as a stationary unit with a main computer and a remote control station.

In longitudinal control, we showed the modeling, design, and simulation of DC motor. In lateral control, the vehicle is controlled by a gyroscope and an ultrasonic sensor, and PID control was designed for reducing a steady-state error, rising time, and overshoot in a velocity control of the vehicle's traction system. We showed the analysis and experiment of the gyroscope's character used for lateral control of vehicle, and the steering system was modeled and controlled through experimental parameter tuning. The performance of the system was evaluated through a simulation program. Also, we showed the analysis and signal process of an ultrasonic sensor character used for lateral control of the vehicle and ultrasonic sensors for obstacle detection and collision avoidance. For more precise control, analysis and signal process require a variable experiment method and algorithm development, which will be used for advanced lateral control. This research on obstacle detection and avoidance can be used in places where humans cannot go. This could have a military application: a robot could go in a minefield where it would be very dangerous for humans.

REFERENCES

Dorf, R. C. and Bishop, R. H. (1997). *Modern Control Systems*, Addison Wesley, New Jersey.

Ellis, J. R. (1969). *Vehicle Dynamics and Control*, London Business Book, London.

Franklin, G. F., Powell, J. D. and Emami-Naeini, A. (1995). *Feedback Control of Dynamic Systems*, Addison Wesley, California.

Kim, D. H. (1993). *Basic and Application of a Small Size Motor*, Jin Young Press, Seoul, Korea.

Kim, M. S. (2001). *The System Modeling for Unmanned Vehicle & Autonomous Driving Technique by Ultrasonic Sensors*, Masters Thesis, Graduate School of Automotive Engineering, Kookmin University, Seoul, Korea.

Kim, B. G., Park, Y. H., Kim, S. G. and Kim, J. H. (2001). The development of collision avoidance algorithm for unmanned vehicle using ultrasonic range sensors. *Proceeding of ICCAS*, Cheju Island, 20–23.

Lee, J. W. (1999). An application of computer vision and laser radar to a collision warning system. *Trans. KSAE* **7, 5**, 258–267.

Lee, S. J. and Yi, K. S. (2001). Throttle/brake combined control for vehicle-to-vehicle distance and speed control. *Trans. KSAE* **9, 2**, 137–142.

National Instruments. (1996). *Lab-VIEW Data Acquisition Basics Manual*, National Instruments Cor., U.S.A..

Paresh, C. S. (1998). *Principles of Electric Machines and Power Electronics*, SciTech Media, Korea.

Park, K. H., Heo, S. J., Paik, I. H. and Yi, K. S. (2001). Estimator design for road friction coefficient and body sideslip angle for use in vehicle dynamics control systems. *Trans. KASE* **9, 2**, 176-184.

Thomas, D. Gillespie. (1992). *Fundamentals of Vehicle Dynamics*, Society of Automotive Engineers, Inc., Warrendale.

Tumbo, S. D., M. Salyani J. D. (2001). Laser, ultrasonic and manual measurements of canopy volumes of citrus trees. *American Society of Agricultural Engineers* (ASAE), *Paper No.* 01-011068.